Raman scattering studies of heavily doped microcrystalline porous silicon and porous silicon free-standing membranes

Dorra Abidi,[1,2] Bernard Jusserand,[1] and Jean-Louis Fave[1]
[1]*INSP, UPMC Université Paris 06, CNRS UMR 7588, 140 rue de Lourmel, 75015 Paris, France*
[2]*Unité Matériaux Avancés et Optronique, Faculté des Sciences de Tunis, 1008 Campus Universitaire Tunis, Tunisia*
(Received 12 February 2010; revised manuscript received 5 July 2010; published 31 August 2010)

The phonon confinement model is often used to analyze Raman scattering band shapes of porous silicon and hence to determine the size of crystallites embedded in the porous layer. We show in this paper, from back-scattering Raman spectra, the importance to avoid using resonant excitation which would select a particular size of nanocrystals. In nonresonant conditions, and working on free-standing porous silicon membranes, broader and more realistic size distributions are found. The disappearance of Fano effect evidences the loss of free carriers in the porous layer. Raman intensity angular variations in parallel and perpendicular polarization configurations are obtained and discussed. They show the presence of unexpected different constant offsets for these two configurations. By comparing with theoretical calculation we deduce that they sign the impact of the porous layer on the light propagation.

DOI: 10.1103/PhysRevB.82.075210 PACS number(s): 61.43.Gt, 78.30.−j, 78.67.Bf

I. INTRODUCTION

Raman scattering has become a standard tool to study the nanostructure of porous silicon, providing an estimation of the characteristic dimensions of Si crystallites in porous layers. The analysis is mainly based on the phonon confinement model[1–3] in which the finite crystallite size is taken into account by weighting the phonon-scattering efficiency. The $q=0$ selection rule is thus relaxed so that the line shape of the first-order phonon peak (near 520 cm^{-1}) is shifted towards lower energies and progressively displays an asymmetric broadening when the crystallites characteristic sizes decrease.

The Raman scattering experiments on this material can, however, suffer from some flaws. Most of the time, the porous layer is not separated from the substrate, which means that a possible significant contribution from the bulk Si should not be disregarded. When strongly absorbed wavelengths are used,[4,5] this contribution is minimal, at least for sufficiently thick porous silicon layers. Furthermore, these excitation energies are resonantly exciting Si-Si vibration in Si nanocrystallites for a well definite size range, giving an explanation to the similar size distributions found in various publications[3–6] but not a real insight on the complete size distribution. In such conditions, a global picture of the porous silicon nanostructure is far to be obtained. Finally heating effects can distort the experimental results and affect the conclusion.

These observations suggested us to use excitation wavelengths out of the resonance range, i.e., red excitation. In addition to the absence of size selectivity, this will minimize sample heating thanks to the weak absorption at this wavelength. Yet, two new features will have then to be considered: the contribution of the signal coming from the substrate and the strong disturbance of the Raman line shape due to the Fano effect in heavily doped silicon.

Indeed, the interaction of electronic Raman transitions with discrete optical phonons results in Fano interference[7] of the first-order Raman scattering. The scattering properties of heavily doped monocrystalline,[8,9] polycrystalline[10–12] silicon, and silicon nanowires[13] have been studied for a long time to probe this effect. However, in our knowledge, the Fano distorsion for porous silicon structures is discussed here for the first time. With increased dopant concentration Raman peak shifts to lower wave number and, depending of the dopant type, severe asymmetries of Raman band occur. Probing the sample using several excitation energies is a powerful method to study this type of phenomenon. Cerdeira *et al.*[8] measured p^+-type silicon using different excitation wavelengths and found that the shape of the Raman spectra changed strikingly with the excitation. Nickel *et al.*[10] performed measurements on *n*- and *p*-type polycrystalline silicon and showed that the variation in the average grain size had no effect on the Fano resonance observed on the Raman spectra.

Thus, to sum up, in the absorption wavelength range, the information on porous silicon nanostructure obtained from Raman excitation can hardly be complete, but in the off-resonance range, analysis could be blurred by Raman scattering from the substrate and asymmetries due to Fano resonance. Aiming to have more comprehensive information about the nanostructure of this material, and to unravel the interferences between the different sources of shift, broadening and asymmetry of the Raman peak, we present in this paper a Raman study of heavily boron and phosphorous doped monocrystalline porous silicon layers (PSLs) and free-standing porous silicon membranes (FSPSMs) using several excitation wavelengths.

After the description of PSLs formation process and experimental setup for Raman scattering (Sec. II), we discuss the transmission spectra for p^+- and n^+-type FSPSMs (Sec. III A). This allows delineating regions of weak and strong absorption bringing about, respectively, nonresonant and resonant Raman scattering conditions. In Sec. III B, we compare results on PSLs and FSPSMs for different excitation wavelengths ranging from resonant to non resonant domains. In nonresonant Raman conditions we will show that it is mandatory to use FSPSM to get significant results (Sec.

 ©2010 The American Physical Society

III C). Finally (Sec. III D), we investigate the angular dependence of Raman scattering intensity by rotating the FSPSM relatively to the polarizations of excitation and detection.

The discussion (Sec. IV) sums up these different experiments and points out specific results concerning conductivity, microstructure, and light propagation in porous silicon layer.

II. EXPERIMENT

PSLs were prepared by electrochemical etching of (001) monocrystalline silicon.[5] We use two types of wafers: a highly phosphorous doped wafer (n^+ type) with a resistivity of 0.002–0.003 Ω cm and a highly boron doped wafer (p^+ type) with a resistivity of 0.001–0.007 Ω cm. The anodization of n^+-type Si was made in HF (40%)-ethanol mixture (5:3 by volume) for 60 s under a current density of 250 mA cm^{-2}, which leads to porosity of 60% and thickness of 10 μm. The electrochemical etching of p^+-type Si was made in HF (40%)-H_2O mixture (1:1 by volume), for 120 s, under a current density of 40 mA cm^{-2}, which gives porosity of 80% and thickness of 3 μm. The process was performed in the dark. The porosity and thickness were obtained gravimetrically.

The morphology of such layers (p^+ and n^+ types) is well characterized in the literature especially by transmission electron microscopy (TEM) (Ref. 14) and scanning electron microscopy (SEM).[15] We report in Figs. 1(a) and 1(b) typical cross-section TEM micrographs of the PSLs used here. Samples for TEM measurements were prepared in the same manner as in the Ref. 5. It can be seen that, whether for the p^+ or n^+ type, the morphology of the layers is very similar. The pores form channels with numerous side branches and their propagation occurs only along the [100] direction.

The insets of Fig. 1 show the plan views of the PSLs. The pore sizes (white areas) were measured directly from the micrograph. They range from 35 to 130 nm with a mean value equal to 65 nm for p^+ sample and from 5 to 35 nm with a mean value equal to 12 nm for n^+ sample. From this micrograph, it is impossible to distinguish the silicon nanocrystallites themselves in aim to estimate their sizes. It simply can be inferred, from the wall thicknesses, that some nanocrystallites can have characteristic sizes as small as about 5 and 7 nm for p^+ and n^+ type, respectively.

Yellow-brown free-standing porous silicon membranes are separated from the Si wafer by electropolishing. The membranes have the same characteristics in terms of porosity and thickness as the porous layers described above, namely, 60% and 10 μm for n^+ type and 80% and 3 μm for the p^+ type. Once detached from their substrates, the membranes are rinsed in ethanol and deposited on quartz plates, on which they adhere perfectly, thanks to the capillarity effect. Thin membranes are very difficult to handle but more the membrane gains in thickness more its handling becomes easy. The etched side looks shiny and highly reflecting while the back side (removed from the wafer) looks dull and rather rough. SEM study[16] confirms that the shiny side shows a very smooth surface while the back side is found to be rough.

The transmission spectra are collected on FSPSMs with UV-Vis spectrometer (CARY 5000 from VARIAN), under atmospheric pressure and at room temperature. The Raman scattering measurements were performed on bulk silicon, PSLs and FSPSMs in a quasibackscattering geometry. Several excitation wavelengths were used in the measurements: 488 nm from an Ar-ion laser, 647 nm from a Kr-ion laser, and 750 nm from a titanium:sapphire laser pumped with an Ar-ion laser. For the 488 nm and 750 nm excitations, Raman spectra were recorded using a DILOR XY 800 monochromator and a cooled charge-coupled-device array with a resolutions of 2.5 cm^{-1} and 0.5 cm^{-1}, respectively. For the 647 nm line, Raman spectra were measured using a Jobin Yvon U1000 and a photomultiplier, with a resolution of 1.5 cm^{-1}. In all the cases the scattered light was collected in the direction normal to the sample surface (001).

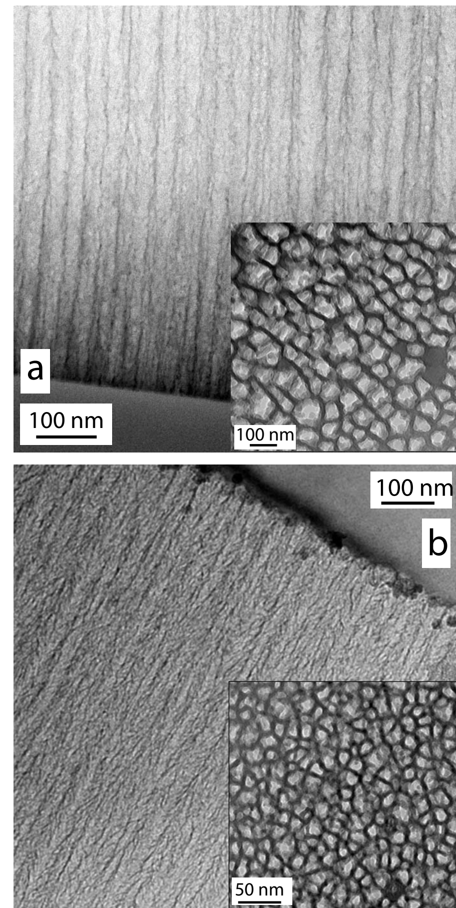

FIG. 1. Cross-sectional TEM micrographs of the porous silicon layers (a) p^+ type and (b) n^+ type. The insets show the plan views.

For bulk Si and PSLs, the orientation of the crystalline axes is perfectly known from the cleavage directions. We place the sample so that one of the crystalline axes [100] or [010] is vertical (it is also the permanent orientation of the analyser in front of the spectrometer). A half-wave plate sets the excitation line polarization, parallel (PA), noted $z(xx)\bar{z}$, or perpendicular (CR), noted $z(xy)\bar{z}$, to the scattered light one. According to the selection rules, in this case the intensity of the scattered light polarized in PA should equal zero.[17] The FSPSMs are removed from the support as fragments so the cleavage directions are no longer identifiable and crystalline Si orientation is not so straightforward; consequently, a sys-

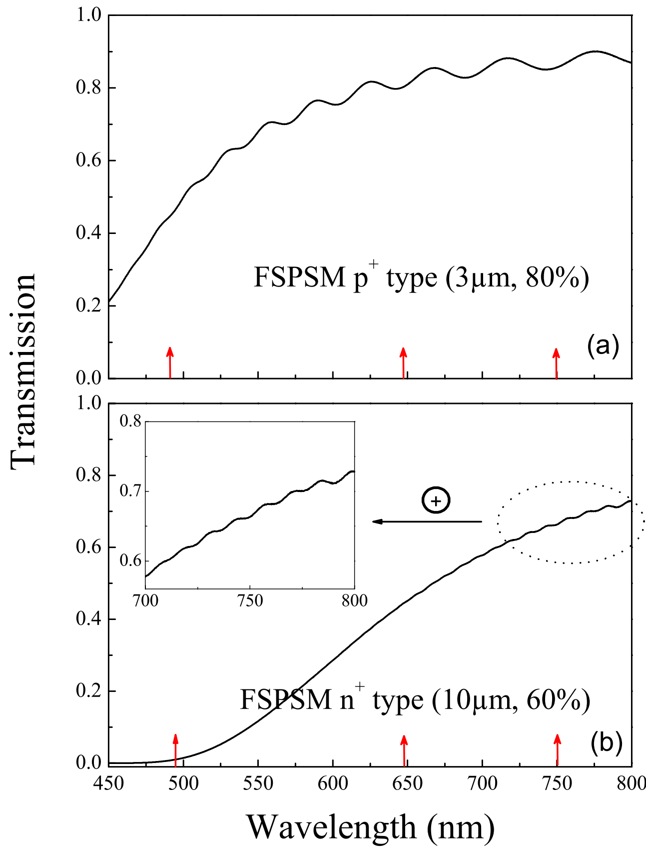

FIG. 2. (Color online) Optical transmission spectra of the free-standing membranes (a) p^+ type and (b) n^+ type. Inset: magnification of the 700–800 nm region.

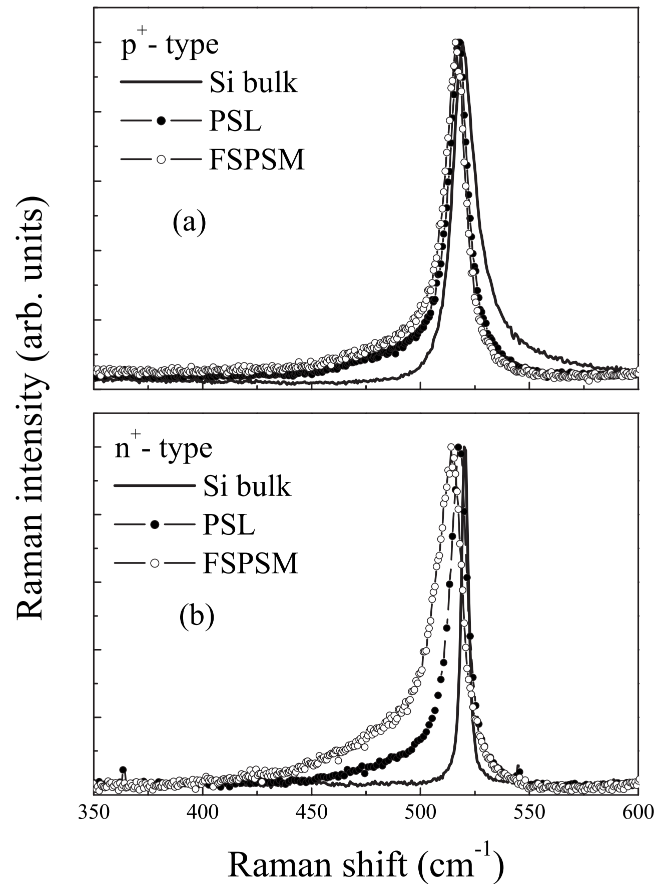

FIG. 3. Raman line shapes for 488 nm scattering wavelength for (a) p^+ type and (b) n^+ type. The bulk Si (solid line), the PSL (solid circle), and the FSPSM (open circle) have been normalized. Bulk Si and PSL spectra are recorded in perpendicular polarization $z(xy)\bar{z}$, contrary to the FSPSM which is not oriented.

tematic study will be necessary to recover the axes directions by rotating the sample in its plane and analyzing the polar plot of the scattered light.

Because of the low thermal conductivity of porous silicon and the temperature dependence of the Raman shifts and line widths, we take care to avoid sample heating and degradation as much as possible by using a line focus to minimize laser power density. All measurement are performed at room temperature

III. RESULTS

A. Transmission

In order to study the Raman spectra evolution according to the excitation energy, we will use laser beams at 750, 647, and 488 nm, ranging from weakly to strongly absorbed (Fig. 2); these excitation wavelengths are pointed out by arrows. Figures 2(a) and 2(b) show the optical transmission spectra in the visible for self-supported membranes p^+ type and n^+ type, respectively. A gradual decrease in the transmission is observed between 800 and 500 nm.

However, the precise quantification of the absorption is difficult because of photon round trips inside the porous layer and the presence of some light diffusion. Moreover, the backside reflection is depending on the interface nature: with air for FSPSM or bulk silicon for PSL. A more complete method to check the optical properties of porous silicon could be a study of the reflectivity.[18,19]

The lack of precision on the absorption coefficient values has no consequence in the present case on the nonresonance-resonance delimitation, which is a function of the size dependent nanocrystallites electronic structure: excitation at 750 nm is clearly weakly resonant.[20] Moreover this measure shows that depending on the wavelength and on the porous layer thickness, more or less beam intensity will reach the substrate. Optical absorption spectra can be also measured directly by photodeflection spectroscopy as reported in Ref. 21.

B. Resonant Raman conditions and wavelength dependence

Raman spectra measured at 488 nm on bulk Si, porous silicon layers, and free-standing porous silicon membranes of heavily boron and phosphorous doped monocrystalline Si are shown in Figs. 3(a) and 3(b), respectively. The p^+-type bulk Si Raman peak centred at 519.4 cm^{-1} is slightly asymmetrically broadened on the high-energy side with a FWHM of $w=13\ \text{cm}^{-1}$ (Table I); this is due to Fano effect.[8] p^+-type PSL and FSPSM Raman spectra are practically identical; they both show an asymmetric broadening on the low-energy

TABLE I. Raman Scattering experiments results with 488 nm excitation.

	p^+ type			n^+ type		
	Bulk	PSL	FSPSM	Bulk	PSL	FSPSM
Raman position (cm^{-1})	519.4	517.4	516.0	520.4	518.0	514.7
FWHM (cm^{-1})	13.0	11.2	12.2	3.5	10.2	16.5
Porosity (%)-thickness (μm)		80-3			60-10	
Estimated transmitted intensity in FSPSM (%)		43			2	

side and a downshift of the phonon frequency towards lower energy by 2 cm^{-1} for PSL and 3.4 cm^{-1} for FSPSM. These broadening and downshift towards lower energy indicate the presence of nanoscale features of the crystalline structures. From Fig. 3(b), it is also noticed that there is no evidence of amorphous phase at 480 cm^{-1} in the measured Raman spectra of the PSL samples.[22]

In the bulk Si n^+ type, the Raman line is centred at about 520 cm^{-1} with a FWHM around 3 cm^{-1}. n^+-type PSL and FSPSM Raman spectra exhibit, as in the case of p^+ type, a low-energy asymmetric broadening and a downshift towards lower energy by 3 cm^{-1} for PSL and 6 cm^{-1} for FSPSM. These values of downshift and broadening are larger than those of p^+ type. This indicates the presence of smaller nanoscale features in the porous layer microstructure. These measurements are summarized in Table I.

In order to investigate the impact of Raman selectivity at 488 nm we performed Raman measurements at 647 and 750 nm as justified in Sec. III A. We show in Fig. 4 the progressive evolution of Raman spectra from resonance (488 nm) to weak resonance (750 nm) on PSL p^+ type. Results at 647 nm give similar information and will be not described here.

C. Nonresonant Raman conditions

Raman spectra measured at 750 nm of bulk Si, porous silicon layers and free-standing porous silicon membranes of

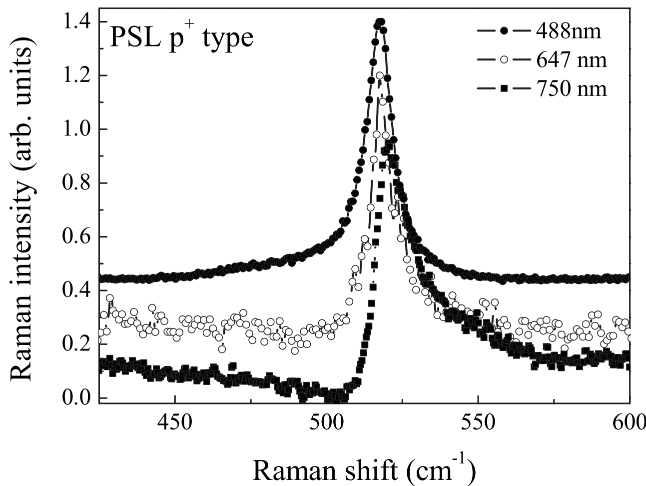

FIG. 4. Raman line shapes for three scattering wavelength: 488, 647, and 750 nm. Spectra are recorded in perpendicular polarization $z(xy)\bar{z}$.

heavily boron and phosphorous doped monocrystalline Si are shown in Figs. 5(a) and 5(b), respectively.

In Fig. 5(a) we can see that bulk Si and PSL Raman spectra are much more distorted than with 488 nm excitation [Fig. 3(a)]. The optical phonon mode is asymmetrically broadened showing a tail situated on the high-energy side of the peak. Either for the bulk Si or the PSL, Raman spectra exhibit a pronounced minimum centred at 507 cm^{-1} besides a maximum at approximately 521 cm^{-1}. This type of line

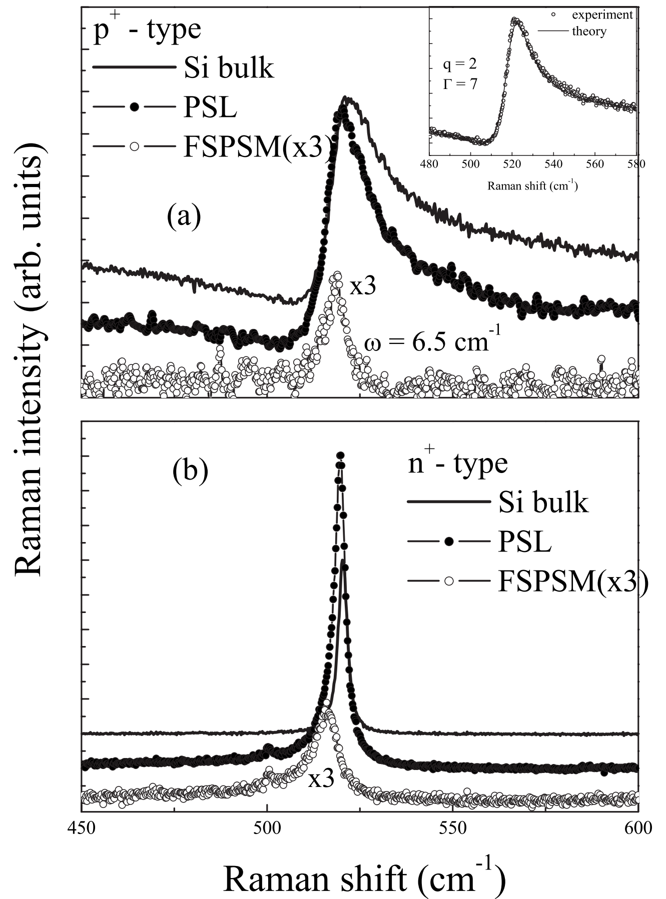

FIG. 5. Raman line shapes for 750 nm scattering wavelength for (a) p^+ type and (b) n^+-type. Bulk Si and PSL spectra are recorded in perpendicular polarization $z(xy)\bar{z}$; for the FSPSM the absolute orientation was unknown. The bulk Si (solid line), the PSL (solid circle), and the FSPSM (open circle) have been shifted vertically with respect to each other. For p^+ type, the base line is defined by the antiresonance minimum. The inset shows the calculation of the Fano line shape for Si bulk p^+ type (Eq. (2)).

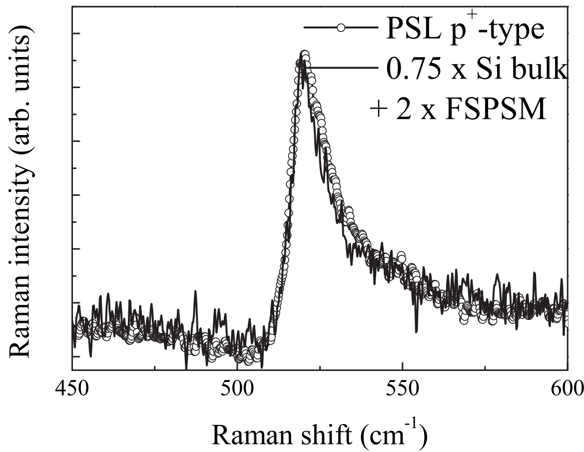

FIG. 6. Raman line shape at 750 nm scattering wavelength of PSL p^+ type (open circle) fitted by the sum of $0.75\times$Si bulk p^+-type $+2\times$FSPSM p^+ type (solid line). PSL and bulk Si (used in the fit) spectra are recorded in perpendicular polarization $z(xy)\bar{z}$; for the FSPSM the absolute orientation was unknown.

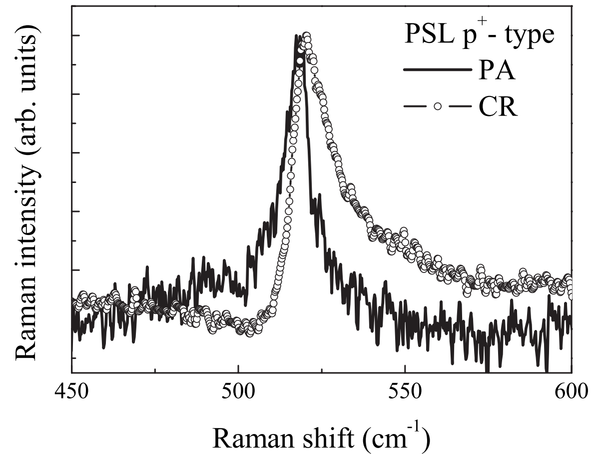

FIG. 7. Raman spectra of PSL p^+ type in parallel configuration (solid line) and perpendicular configuration (open circle). The excitation frequency is 750 nm.

shape is well known as a Fano resonance[7] and has been extensively studied in heavily doped monocrystalline,[8,9] polycrystalline[10–12] silicon, and silicon nanowires[13] and also in heavily p^+-type diamond[23] but this is the first time that this phenomenon is discussed on porous silicon layers. However, this distortion disappears completely in the FSPSM p^+-type Raman spectrum and the line shape of the phonon peak, with an asymmetric peak centred at 518.5 cm^{-1} and a full width at half maximum (FWHM) of $w=6.5$ cm^{-1} [Fig. 5(a)], becomes indeed closer to the PSL Raman shapes usually reported for visible excitation[2,3,5] and shown in Fig. 4 for our sample.

Figure 5(b) presents heavily phosphorous doped bulk Si, PSL, and FSPSM Raman spectra. The first-order Raman spectra of bulk silicon shows a perfectly symmetric peak at 520.3 cm^{-1} with FWHM of 2.9 cm^{-1}. But Raman spectra from the PSL and the FSPSM exhibit an asymmetric broadening and a downshift towards lower energy. A larger frequency downshift 4.3 cm^{-1} is noted for the FSPSM and a FWHM of 9.1 cm^{-1}. For PSL the Raman peak moves only by 0.7 cm^{-1} with a FWHM of 4 cm^{-1}.

Returning to the p^+ type [Fig. 5(a)] it is conspicuous that the Raman signal in the PSL is closer to the bulk Si one than to the FSPSM one; indeed, the FSPSM is sufficiently transparent to this excitation wavelength to allow significant contribution of the bulk substrate. From the transmission results (Fig. 2), we estimate that at least 98% of the excitation intensity reaches the bulk. Figure 6 demonstrates that we can reconstruct the PSL Raman spectrum from bulk Si and FSPSM signals via a simple weighted summation. The solid line curve is generated without taking into account the crystalline axes orientation of the FSPSM. Indeed, we will show in Sec. III D that only the intensity of the Raman signal changes according to the axes orientation, and that its position and its FWHM remain steadfast. Thus, as far as the fit is concerned, only the weighting coefficient will change. Consequently, the decomposition of PSL Raman on $0.75\times$Si bulk $+2\times$FSPSM remains valid. A similar reconstruction of the PSL Raman spectrum, was made at 647 nm using a simple weighted summation (not shown); $0.5\times$Si bulk $+0.5\times$FSPSM gives a good agreement.

D. Polarization

All the experiments described until now were performed in crossed polarization in which the bulk Si Raman signal is allowed; we will show first that using parallel polarization allows to cancel the bulk signal and to access to the pure porous silicon signal. Figure 7 shows normalized Raman spectra of the PSL p^+ type in PA and CR polarization with [100] axis vertical. It is clear that the two spectra are completely different. In CR configuration, due to the weak absorption of the porous layer, the Raman spectrum arises essentially from the bulk Si. But in PA configuration, selection rules cancel the substrate Raman signal but not the porous layer one. Thus, for this orientation, the PSL p^+-type Raman peak, centred at 517.3 cm^{-1} and with FWHM of 7.5 cm^{-1} corresponds exactly to the FSPSM one [shown in Fig. 5(a)].

Another point of interest is to determine how far the freestanding porous silicon membrane keeps the same crystalline properties than the original wafer. So we investigated the dependence of the Raman peak intensity in PA and CR polarization on the angle β between the [001] axis and the plane of oscillations of the electric field vector of the light both for the FSPSM p^+ and n^+ type. The angle $\beta=0$ corresponds to a position chosen arbitrarily at the beginning of the measurements. The Raman spectra line shape does not vary with β. The Raman intensity $I(\beta)$ is determined after subtraction of the baseline which was found unpolarized. Figure 8 shows the angular dependences $I(\beta)$ obtained in parallel polarization and in perpendicular polarization in polar graph. We determine from this figure that the crystalline axes are at about 13° and 57° for p^+ and n^+ type, respectively. The polar diagrams display the characteristic clover leaves shape anticipated for Si (001) plane.[24] However, at the reverse of bulk crystal, the diagrams in PA and CR polarization are very different in intensities. Indeed, in parallel polarization we note an unexpected feature: the lobes are superimposed on an

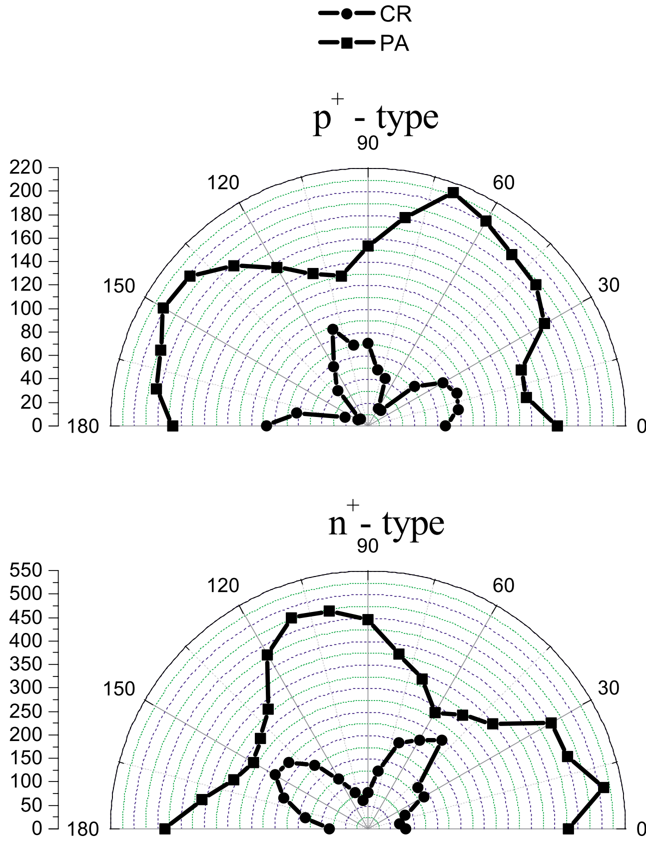

FIG. 8. (Color online) Degree of linear polarization of Raman scattered light versus the β angle between the [001] axis and the plane of oscillations of the electric field vector of the excitation light for the FSPSM p^+ type and n^+ type in parallel polarization (solid square) and in perpendicular polarization (solid circle). The excitation frequency is 750 nm

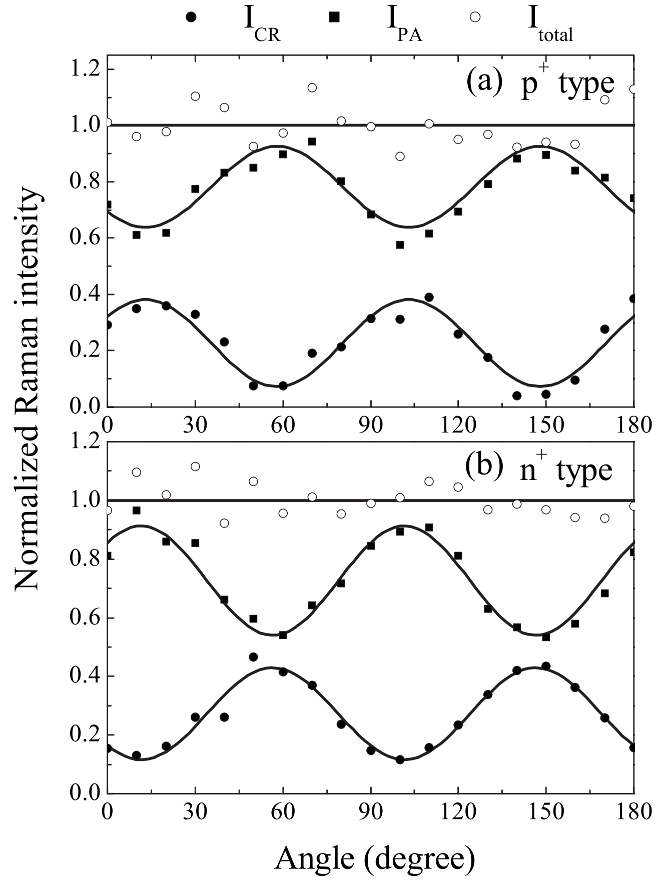

FIG. 9. Experimental angular variations in normalized Raman intensities for (a) p^+ type and (b) n^+-type porous silicon membrane (same data as Fig. 8). The solid lines highlight the expected sinus laws.

important constant offset. We have verified that this offset is not an experimental artifact but a real signal originating from the sample.

IV. DISCUSSION

Our experimental results show some unexpected features for the line shapes and angular dependence of PSL and FSPSM Raman spectra. In this section we will discuss them with the objective to draw the best possible information on the microstructure.

A. Polarization behavior of Raman spectra

The polar diagrams of backscattered Raman emission [intensities depending of the rotation β of a separated porous membrane between crossed or parallel polarizers (Fig. 8)] show clearly an important deviation relatively to the classic and expected behaviour of a Si (001) crystal plane.

Once normalized to the angular average of $I_{PA}+I_{CR}$ and displayed in Cartesian coordinates (Fig. 9), the same experimental angular variations expose even better very distinctive features: (a) $I_{PA}+I_{CR}$ have the same value for any orientation β; (b) the angular variations follow nicely $\sin^2 2\beta$ and $\cos^2 2\beta$ laws, of same amplitudes but they are superimposed on a constant term which is larger for PA configuration; (c) the outlook is the same for the two types of doping.

The origin of this behaviour could be searched in the microstructure of the porous layer and its effect on light propagation. We will begin with three relevant observations: (i) in our experiments, the excitation beam goes through the layer without significant depolarization, as it is shown by the complete extinction of the substrate Raman signal for polarizers parallel to the [001] crystal axis on supported porous layer (Fig. 7); there is also the same evidence from transmission experiments through membranes.[24] Furthermore the depolarization would simply mix I_{PA} and I_{CR}, reducing their amplitudes without adding any constant term. (ii) On the other hand, the pores give rise to an uniaxial asymmetry, even if the silicon atoms positions in the porous layer retain the original monocrystalline structure; however, the propagation being a priori along the pores general direction [001], no deviation due to the difference in optical indexes should occur, at least at first glance. (iii) The sizes of nanostructures are small relatively to the wavelength but large enough for some Rayleigh scattering to take place. Scattering of the incoming light in the porous layer leads to light trapping inside the porous layer[25] and increases the probability of Raman scattering at the price of some randomization of the excita-

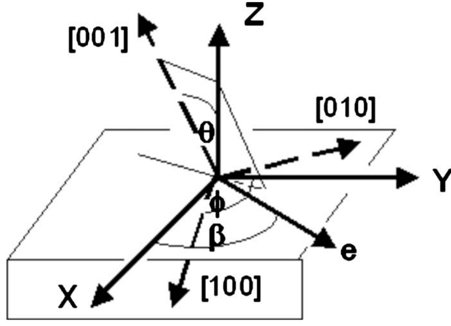

FIG. 10. Raman scattering geometry used in this experiment and relation between laboratory coordinate system and crystal axes system.

tion light. The important consequence is that a part of the Raman signal can be produced by this scattered excitation light; the Raman shifted photons can too undergo scattering before collection.

These remarks point out to go to some extent beyond the description of porous silicon as an homogeneous optical medium,[18] and to consider, in the inverse limit, the porous layer as a collection of distinct scattering centres. This could be justified because, although the scatterers interdistances and sizes are much smaller than light wavelength, they are inhomogeneously arranged, precluding coherence between beams scattered by the different nanocrystals.

The key point is to determine how after scattering the excitation beam impinges on the crystal planes of the different nanocrystals embedded in the pore walls and the resulting effect on the Raman intensity. Mizoguchi and Nakashima[26] investigated the use of Raman microprobe to ascertain orientations of micron-sized Si crystals in backscattering configuration. The Raman intensity is determined by the direction and polarization of incident and scattered beams relatively to the polarizability tensor axis and then its anisotropy provided means to determine crystal orientation (Fig. 10).

Our analytical derivation[27] based on this geometry gives the following results shown in Table II after some averaging on equivalent and indistinguishable orientations. In the general case, θ and ϕ define the propagation direction inside the crystal, relatively to the Raman scattering tensor axis.

Of course, for propagation along such direction as [001], in backscattering configuration, the polar variation involves one component of the polarizability tensor and obeys to $\sin^2 2\beta$ and $\cos^2 2\beta$, for the rotation β between parallel [intensity $I_{PA}(\beta)$] and crossed [intensity $I_{CR}(\beta)$] polarizers, respectively. This is the case of the wafers we use as substrates [Fig. 11(a)].

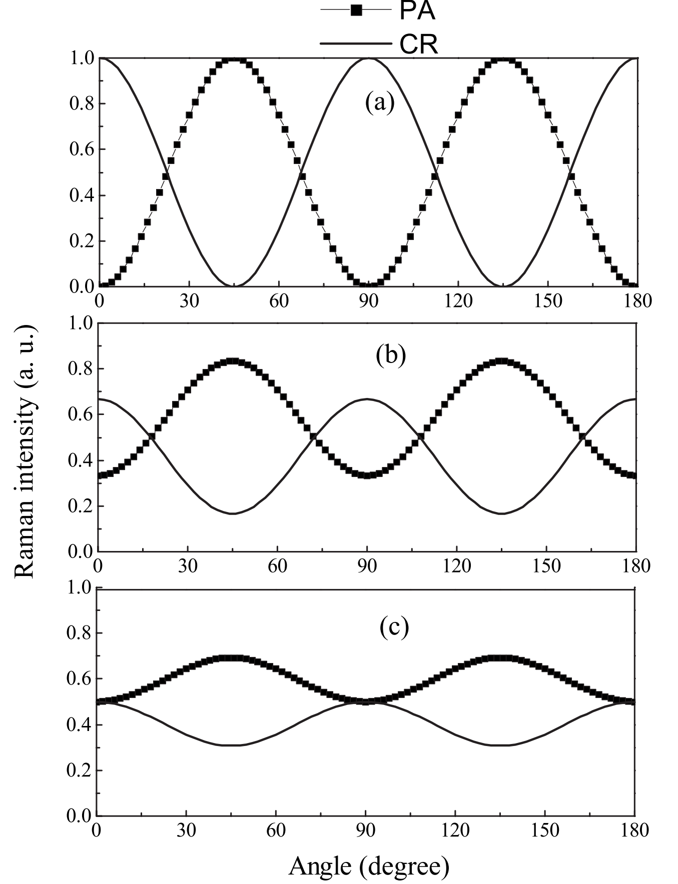

FIG. 11. Normalized angular variation in I_{PA} and I_{CR} for: (a) plane (001), (b) family of planes (101), and (c) family of planes (111).

In general, for propagation tilted by $\theta°$ from [001] and orthogonal to (0n1) or (n01) planes, the two branches vary differently, as

$$I_{PA}(\beta) = \sin^2 2\beta\left(1 - \frac{1}{4}\sin^2 2\theta\right) + \frac{1}{2}\sin^2 2\theta,$$

TABLE II. Analytical expression of Raman intensity in the two configurations.

Conf.	PA	CR
$I_{conf}(\beta)$	$\left(\frac{\sin^2\theta\sin 2\phi}{2}\right)^2 + \left[\frac{(1+\cos^2\theta)}{2}\sin 2\phi\cos 2\beta + \cos\theta\cos 2\phi\sin 2\beta\right]^2 + 2\sin^2\theta\cos^2\theta + \sin^4\theta\sin^2 2\beta$	$\left[-\frac{(1+\cos^2\theta)}{2}\sin 2\phi\sin 2\beta + \cos\theta\cos 2\phi\cos 2\beta\right]^2 + \sin^2\theta\cos^2\theta + \sin^4\theta\cos^2 2\beta$
I_{tot}	$\sin^2\theta(1+2\cos^2\theta) + \frac{(1+\cos^4\theta)}{2}\sin^2 2\phi + \cos^2\theta\cos^2 2\phi$	

$$I_{\mathrm{CR}}(\beta) = \cos^2 2\beta\left(1 - \frac{1}{4}\sin^2 2\theta\right) + \frac{1}{4}\sin^2 2\theta \qquad (1)$$

whose the sum $1+1/2\,\sin^2 2\theta$ is indeed independent of the rotation angle. The symmetry is kept, with different offsets for PA and CR polarizations [Fig. 11(b)].

Indeed these results (symmetry, offset) hold for any propagation direction [Fig. 11(c)] but not to the extent where the two branches would not intersect, as in the experimental results, even by combining and averaging different orientations. So that these results show mainly that the propagation direction in nanocrystals is probably not only along the [001] axis, compelling us to consider that the signal results from a complex average over the different nanocrystals but constrain too to search for other contributions to explain the offsets.

One first effect could be due to the shape of the nanocrystals: columns, spheroids, and platelets have been proposed. The excitation beam impinging on a tilted facet of a nanocrystal would be refracted (as far as refraction as a clear meaning, due to the small size of the microstructures) and would propagate along a particular direction and eventually give rise to Raman scattering. Owing to the geometry of the set up, the collected beam can consist of photons following the exactly reverse path, i.e., being strictly collinearly backscattered but has a chance too to contain scattered photons exiting through another facets and refracted parallel to the excitation beam. This last possibility escapes to our present calculation but some inkling can be found in experiments dealing with the angular dependence of Raman intensities for a collection of randomly oriented scattering centers.[28] The depolarization ratio ($I_{\mathrm{CR}}/I_{\mathrm{PA}}$) of amorphous silicon for the vibration mode of the same cubic symmetry is about 0.5.[29] Indeed, by taking into account a ratio of random scattering, different constant terms are added to $I_{\mathrm{CR}}(\beta)$ and $I_{\mathrm{PA}}(\beta)$. However, this value of the depolarization ratio is too large to cope with our experimental data, it is only tentative because a complete propagation randomness is far to be demonstrated. Finally one can conclude from experiment that less porous sample n^+ exhibits larger modulation amplitude, which is consistent with our interpretation (Fig. 9).

At last, x-ray investigations of the porous silicon microstructure show the existence of strain and mosaicity which can distort and disorient unit cells. This would make necessary to modify the polarizability tensor components and to sum up the Raman scattered intensities on distribution of angles around β, θ, and ϕ (Table II), with likely modification of the offsets and decrease in modulation amplitudes of $I_{\mathrm{CR}}(\beta)$ and $I_{\mathrm{PA}}(\beta)$. Actually reported results suggest that mosaicity and strain are rather weak,[30,31] so that their eventual consequence on polar diagrams will be limited.

To summarize, the analysis of the angular variation in the collected Raman light shows it can not result from strictly backscattered radiation but includes components scattered in other directions. Indeed, the presence of silicon nanocrystals embedded in the walls creates local inhomogeneity of structure so that excitation light is not compelled to propagate in Si along the crystal axis, i.e., along the axis of the polarizability tensor; this out of axis part of excitation beam can gives rise to Raman scattering. A detailed knowledge of the distribution of these propagation directions relatively to the crystal axis would be needed to give a more quantitative account for the observed modulation.

B. Free carriers in porous silicon

The phonon peak characteristic observed on the bulk Si and PSL spectra of heavily boron doped monocrystalline Si can be explained by the Fano effect.[8] It is a general effect arising from the interaction between the optical phonon scattering (discrete) and direct intraband transitions of charge carriers (continuous). Fano first proposed this mechanism to explain asymmetries in atomic absorption spectra.[7] The Raman scattering cross section (Fano profile) can be described by

$$F(\omega) = \frac{[q + \varepsilon(\omega)]^2}{1 + \varepsilon(\omega)^2},$$

$$\varepsilon(\omega) = \frac{\omega - \omega_p}{\Gamma}, \qquad (2)$$

where q is the symmetry parameter, ω is the measured frequency, ω_p is the phonon frequency, and Γ is the linewidth contribution to the total linewidth. q and Γ are the curve-fitting parameters. According to the sign of q one can determine on which energy side the light-scattering rate is enhanced.

Cerdeira *et al.*[8] were the first to use the Fano effect to explain the optical phonon line shape of heavily doped c-Si. It is based on the existence of continuum of Raman-active electronic excitations produced by intravalence-band transitions, whose energy overlaps with that of the optical phonon. In the case of silicon, such Fano line shape occurs when the Fermi energy shifts into the conduction or valence band consequently to the high concentration of free charge carriers into the material. Our p^+-type Si wafers are of resistivity $0.001-0.007\ \Omega\,\mathrm{cm}$ which corresponds to a free hole concentration of $1.16\times10^{20}\ \mathrm{cm}^{-3}-0.13\times10^{20}\ \mathrm{cm}^{-3}$.[32] These values are sufficient to move the Fermi energy into the valence band at room temperature. Using Eq. (2), the p^+-type bulk Si Raman backscattering spectra shown in Fig. 5(a) can be fitted. The fitting results are shown in the inset of Fig. 5(a). The values found for the symmetry parameter q and the linewidth contribution to the total linewidth Γ are in good agreement with the values found in literature.[8,33]

As we can note in Fig. 5(a), the FSPSM p^+-type Raman spectrum does not show in no way this Fano line shape. This is certainly related to the free-carrier concentration. Indeed, dopants in porous silicon have been deeply investigated, particularly by Grosman and Ortega.[34] They discuss several explanations for the weak conductivity of PSL: (i) the absence of dopants in porous silicon structure which means that the boron atoms disappeared with the porosification of the wafer. (ii) A possible passivation of boron atoms by hydrogen in the porous structure. (iii) A lack of free charge carriers in the Si matrix. Grosman and Ortega[34] studied in detail, by nuclear reaction analysis, Fourier transformed infrared spectroscopy (FTIR), and electron paramagnetic resonance (EPR), the

dopants in porous silicon and the results are rather interesting. Indeed, according to the sample porosity, the PSL boron atoms concentration is equal to, or even higher than that of the substrate because of the selective electrochemical etching of regions free of dopant,[35] so the first hypothesis is to be rejected. FTIR experiments reveal that dopant atoms are not neutralized by hydrogen in the PSL but that the passivation occurs only at the porous/bulk interface, thus the second hypothesis is also to be rejected. The phenomenon thus seems to be closely related to the trapping of free carriers on surface states. Anderson *et al.*[36] was the first to suggest that the free carriers are trapped on surface states in PSL. Through EPR measurements made on FSPSM and PSL n^+ type, Grosman and Ortega[34] confirm this idea and found that the neutral Si dangling bonds defect are probably responsible of it. Microwave absorption shows the existence of surface states.[37] Under these circumstances, the material behaves as an undoped semiconductor, with no possibility of intraband transition, and the Fano interference disappears.

The a priori surprising observation of a Fano profile in PSL p^+ sample is due to the weak absorption of the porous layer at 750 nm. The Fano shape, clearly seen on the PSL Raman spectrum, is nothing else than the contribution of the bulk. The PSL Raman spectrum can be reconstructed by summing the bulk data and the FSPSM data with weighting coefficients of 0.75 and 2, respectively, as shown in Fig. 3.

Similar phenomenon is also possible for heavily doped n-type silicon.[11] The Fano broadening is weaker in n^+-type monocrystalline Si and of opposite sign. Consequently, the asymmetric broadening occurs on the low-energy side of the optical phonon. The Fano line shape for the n^+-type appears clearly only when the phosphorous concentration reaches 10^{20} cm^{-3}. Our Si wafer is of resistivity $2-3\times10^{-3}$ Ω cm which corresponds to a free hole concentration of 3.43×10^{19} cm$^{-3}-2.25\times10^{19}$ cm^{-3}, then these values are not sufficient to observe the resonant interaction between the optical phonon Raman and the electronic Raman, which explains the Fig. 5(b) line shape.

C. Microstructural characterization in and out of resonance

Raman scattering is claimed to be a valuable technique to characterize the porous silicon microstructure. Some cautions have to be taken to get meaningful information. The key point is to minimize the substrate contribution to the Raman spectrum. For this we can excite in or out of resonance (Fig. 4), use a FSPSM (Fig. 3) or take advantage of Raman selection rules (Fig. 7).

According to the study of Cerdeira *et al.*,[8] the Fano effect should decrease with an excitation moving towards high energies. This explains the shape of the bulk Si Raman spectrum in Fig. 3(a), as well as the evolution of Raman spectra on PSL p^+ type (Fig. 4). Thus, out of resonance (Fig. 4) there is no possibility to investigate a PSL except if we are in PA polarization (Fig. 7). The obvious way to study a FSPSM is also possible (Fig. 5). Indeed, PSL p^+-type Raman spectrum in PA configuration and FSPSM p^+-type Raman are identical as demonstrated in Sec. III B.

Table I shows that more than 50% of the excitation energy at 488 nm is absorbed by the porous layer p^+ type, which explains why we do not distinguish the contribution of the bulk Si as in Fig. 5(a). Thus, in strongly resonant Raman conditions, PSL and FSPSM should give the same spectra in terms of peak position and FWHM. This is almost true for p^+ type (Table I) but for n^+ type it is clearly different. The peak position of the FSPSM n^+ type is shifted by 3.3 cm^{-1} compared to the PSL one and the spectrum is 1.6 times wider. This is probably due to the heating of the sample. Despite the cautions taken, it seems that the FSPSM n^+ type overheats dramatically inducing the broadening and the shift of the spectrum (the major part of the excitation energy is absorbed, Sec. III A).

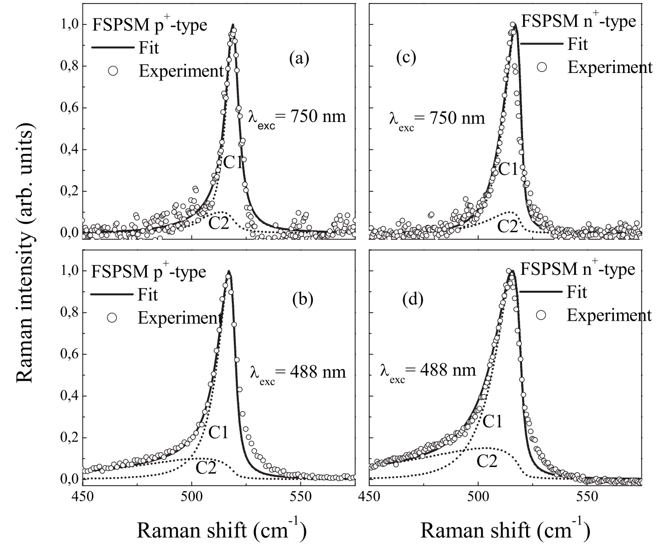

FIG. 12. Measured Raman spectra (open circles) on a FSPSMs samples along with fitted data (solid line). Spectra (a) and (b) show p^+ type, spectra (c) and (d) show n^+ type. A Gaussian distribution in crystallite sizes occurs with two nanocrystalline components C_1 and C_2. The fit parameters R_0 and σ are shown in Table III.

In order to determine the crystallite size distribution (CSD) in our structure, we adopt the model proposed by Islam and Kumar[3] which shows an explicit inclusion of a Gaussian CSD to calculate the Raman spectra of porous silicon. Reference 5 details all the steps of calculation and the fit procedure. The fits realized on p^+ and n^+ FSPSMs and presented in Fig. 6 show that, in all cases, two Gaussian components are sufficient to describe the data: C_1 which refers to the large dimensions and C_2 which represents crystallites of

TABLE III. Nanostructural parameters from Raman Scattering experiments.

		FSPSM p^+ type		FSPSM n^+ type	
		R_0 (nm)	σ (nm)	R_0 (nm)	σ (nm)
488 nm	Component C_1	7.0	1.3	5.0	0.70
	Component C_2	2.2	0.1	2.2	0.35
750 nm	Component C_1	15.0	3.1	6.0	0.50
	Component C_2	4.0	0.1	1.0	0.10

smaller size, scattering more efficiently and responsible for Raman line shift and broadening (Fig. 12).

Table III summarizes the best fit results for both p^+ and n^+ FSPSMs in and out of resonance. R_0 is the mean crystallite size and σ is the standard deviation of the Gaussian size distribution given here in fraction of R_0. For p^+ type, the crystallite size values R_0 are larger and the distributions are wider at 750 nm than at 488 nm, which indicates that the photoselection phenomenon detected when we use a strongly absorbed excitation becomes clearly less intense when the excitation frequency is weakly absorbed. For n^+ type, the fit has a lower quality in the two cases and the results are less revealing owing to the probable overheating of the sample.

The TEM images and the Raman lineshape analysis give complementary information on the crystallites structure. The Raman analysis is based on phonon confinement in spherical crystallites while the wall thicknesses deduced from TEM images (5 nm for p^+ and 7 nm for n^+) reveal only the smallest dimension of the embedded nanocrystals.

V. CONCLUSION

Raman scattering is one of the few methods that allow characterizing Si crystallites remaining in the porous layer, usually by using the phonon confinement model to estimate the sizes of existing crystallites. Despite its appeal, such a study is not easy to achieve and the choice of the excitation frequency is crucial for the quality of results. Indeed, a photoselection phenomenon appears when using excitation wavelength close to the absorption edge of some of the nanocrystallites embedded in the porous silicon layer. This prevents to have a real insight on the complete size distribution. To overcome this limitation, we show the advantage of exciting outside the absorption band of the PS. However, this brings up some issues since the substrate signal can be collected with the porous silicon one and causes some distortion. This problem can be circumvented by: (1) using FSPSM; (2) using Raman selection rules to filter out the additional substrate signal on a PSL sample.

From there we have shown that the Fano effect, prevalent in highly doped bulk Si, disappears with porosification of the substrate; which means that porous layers are free of mobile carriers, confirming former studies made by other methods. This could open a new way to access to the conductivity and its variation as for example when it is restored by exposition to nitrogen dioxide NO_2,[38] or by annealing in nitrogen ambience for a short period.[12]

Once we are out of photoselection conditions and free from Fano effect, it becomes possible to assume the accuracy of the experimental Raman lineshape, a very simple and nondestructive technique. However, the microstructural analysis by the phonon confinement model is based on spherical crystallites and, although we found admissible parameters, more work is needed on this point to compare to HRTEM determination of size distribution.[39]

When detached from the substrate, the FSPSM orientation is lost. We show that we can recover the axis directions by studying Raman intensity angular variation in parallel and perpendicular configurations. Furthermore the experience shows the presence of unexpected different offsets for these two configurations. From comparison with theoretical calculation of backscattered Raman intensity we infer the excitation beam is not compelled to propagate only along the crystal axis, i.e., along the axis of the polarizability tensor. But, at our current understanding level, it is not possible to explain quantitatively the observed offsets.

A more comprehensive view could be obtained through a study based on samples of various porosities in different Raman excitation and collection geometries to have a better understanding of the origin of these constants, with the hope to find a link to the form and size of nanocrystals in porous silicon.

ACKNOWLEDGMENTS

The authors are very grateful to A. Grosmann, J. F. Morhange, T. Barisien (INSP), S. Romdhane (FSB) for their help in samples preparation, experiments, and discussion and D. Demaille (INSP) for TEM characterizations. Financial support for this work was provided by the ″Comité Mixte de Coopération Universitaire Franco-Tunisien″ Project No. 05S1304.

[1] H. Richter, Z. P. Wang, and L. Ley, Solid State Commun. **39**, 625 (1981).
[2] I. H. Campbell and P. M. Fauchet, Solid State Commun. **58**, 739 (1986).
[3] Md. N. Islam and S. Kumar, Appl. Phys. Lett. **78**, 715 (2001).
[4] B. K. Patel, R. Mythili, R. Vijayalaxmi, R. K. Soni, S. N. Behera, and S. N. Sahu, Physica B **322**, 146 (2002).
[5] D. Abidi, S. Romdhane, A. Brunet-Bruneau, and J.-L. Fave, Eur. Phys. J.: Appl. Phys. **45**, 10601 (2009).
[6] R. Tsu, H. Shen, and M. Dutta, Appl. Phys. Lett. **60**, 112 (1992).
[7] U. Fano, Phys. Rev. **124**, 1866 (1961).
[8] F. Cerdeira, T. A. Fjeldy, and M. Cardona, Phys. Rev. B **8**, 4734 (1973).
[9] M. Chandrasekhar, J. B. Renucci, and M. Cardona, Phys. Rev. B **17**, 1623 (1978).
[10] N. H. Nickel, P. Lengsfeld, and I. Sieber, Phys. Rev. B **61**, 15558 (2000).
[11] P. Lengsfeld, S. Brehme, K. Brendel, Ch. Genzel, and N. H. Nickel, Phys. Status Solidi B **235**, 170 (2003).
[12] R. Saleh and N. H. Nickel, Surf. Coat. Technol. **198**, 143 (2005).
[13] T. Kawashima, G. Imamura, T. Saitoh, K. Komori, M. Fujii, and S. Hayashi, J. Phys. Chem. C **111**, 15160 (2007).
[14] R. L. Smith and S. D. Collins, J. Appl. Phys. **71**, R1 (1992).
[15] C. Levy-Clement, Porous silicon science and technology, lecture 20, 327–344, Les Editions de Physique-Springer, (1994).
[16] S. Guha, P. Steiner, and W. Lang, J. Appl. Phys. **79**, 8664 (1996).
[17] H. Poulet and J. P. Mathieu, *Spectres de Vibration et Symmetries*

des Cristaux (Gordon and Breach, Paris, New York, London, 1970).

[18] G. Lerondel and R. Romestain, in *Properties of Porous Silicon*, edited by L. Canham (INSPEC, London, 1997), Chap. 8, p. 241.

[19] W. Theiss, S. Henkel, and M. Arntzen, Thin Solid Films **255**, 177 (1995).

[20] I. Sagnes, A. Halimaoui, G. Vincent, and P. A. Badoz, Appl. Phys. Lett. **62**, 1155 (1993).

[21] M. Rosenbauer, M. Stutzmann, S. Finkbeiner, J. Weber, and E. Bustarret, Phys. Rev. B **55**, 10117 (1997).

[22] Z. Iqbal and S. Veprek, J. Phys. C **15**, 377 (1982).

[23] Y. G. Wang, S. P. Lau, B. K. Tay, and X. H. Zhang, J. Appl. Phys. **92**, 7253 (2002).

[24] M. E. Kompan, V. B. Kulik, I. Novak, J. Salonen, and A. V. Subashiev, JETP Lett. **67**, 106 (1998).

[25] P. N. Vinod and M. Lal, J. Mater. Sci.: Mater. Electron. **16**, 1 (2005).

[26] K. Mizoguchi and S.-I. Nakashima, J. Appl. Phys. **65**, 2583 (1989).

[27] D. Abidi, Ph.D. thesis, Université Pierre et Marie Curie (Paris 6) et Faculté des Sciences de Tunis, 2009.

[28] W. Hayes and R. Loudon, *Scattering of Light by Crystals* (Dover, New York, 1978).

[29] M. Ivanda, O. Gamulin, and W. Kiefer, J. Mol. Struct. **480-481**, 651 (1999).

[30] M. Binder, T. Edelmann, T. H. Metzger, and J. Peisl, Solid State Commun. **100**, 13 (1996).

[31] P. G. Abramof, A. F. Beloto, A. Y. Ueta, and N. G. Ferreira, J. Appl. Phys. **99**, 024304 (2006).

[32] National Bureau of Standards Special Publication 400-64, *The Relationship Between Resistivity and Dopant Density for Phosphorus- and Boron-Doped Silicon* (May 1981), Table 10, Page 34 and Table 14, Page 40.

[33] F. Cerdeira, T. A. Fjeldy, and M. Cardona, Solid State Commun. **13**, 325 (1973).

[34] A. Grosman and C. Ortega, in *Properties of Porous Silicon*, edited by L. Canham (INSPEC, London, 1997), Chap. 11, p. 328.

[35] V. M. Dubin, Surf. Sci. **274**, 82 (1992).

[36] R. C. Anderson, R. S. Muller, and C. Tobias, J. Electrochem. Soc. **138**, 3406 (1991).

[37] H. E. Porteanu, Phys. Status Solidi A **204**, 1362 (2007).

[38] E. Garrone, S. Borini, P. Rivolo, L. Boarino, F. Geobaldo, and G. Amato, Phys. Status Solidi A **197**, 103 (2003).

[39] T. L. S. L. Wijesinghe, E. J. Teo, and D. J. Blackwood, Electrochim. Acta **53**, 4381 (2008).